Tomography of cylindrical objects: comparison of noise property and accuracy of Abel inversion techniques with and without noise filtering (published, see [1])

Shuiliang Ma

Plasma Research Laboratory, Australian National University, Canberra ACT 0200, Australia

Abstract

I have analyzed and compared the noise property and accuracy of three kinds of Abel inversion technique, i.e., the polynomial interpolation, versatile polynomial fitting (VPF) and modified Fourier-Hankel (MFH) methods. All these techniques will amplify noise due to the intrinsic property of Abel inversion. A technique that is more sensitive to noise also has a higher inversion accuracy for data without noise. Among the techniques without noise resisting property, the third-degree polynomial interpolation and MFH methods have comparable performance and give higher inversion accuracies than other techniques. The VPF and MFH methods, which can be used without extra filtering of noise, yield markedly better results compared with those obtained by using noise filters in advance of inversion. Both of these two methods can be considered for applying to experimental data if there are no better smoothing techniques available.

1. Introduction

In many areas of physics and engineering, such as plasma diagnostics [2] and combustion research [3], the measured signals are usually the line-of-sight integration of certain physical quantity within the object. To reconstruct the local quantity from experimental measurements, tomography techniques are therefore required. Particularly, for a cylindrically symmetric and optically thin radiation source with radius R, the measured lateral intensities are connected by the radially distributed emission coefficients, which can be described by the forward Abel transform:

$$I(x) = 2\int_x^R \frac{\varepsilon(r)r}{\sqrt{r^2-x^2}}\mathrm{d}r. \tag{1}$$

And the inverse Abel transform for reconstruction of the emission coefficient is given by

$$\varepsilon(r) = -\frac{1}{\pi}\int_r^R \frac{I'(x)}{\sqrt{x^2-r^2}}\mathrm{d}x, \tag{2}$$

where $I'(x) = \mathrm{d}I(x)/\mathrm{d}x$.

In practice, Eq. (2) cannot be directly applied to experimental data because the measured intensities are discrete values and the derivative of the intensity and the singularity in the integration exist, which will greatly amplify the uncertainties in the experimental data, especially for the region close to the source center. To overcome these difficulties, a large number of techniques have been developed over the past years. Techniques based on both Eqs. (1) and (2) have been proposed. Most techniques use Eq. (2) to take the inversion by representing the intensity profile with an analytical function. One of the approaches uses the polynomial interpolation technique [4,5] to approximate the intensity profile. Because this kind of technique does not consider the uncertainties in the intensity data, extra noise filtering should be performed before the inversion. Fitting the intensity profile in the whole interval with a single polynomial [6] will distort the intensity distribution, thus piecewise polynomial least-squares fitting [7–9] has been suggested for achieving a better inversion accuracy. Other techniques such as representing the intensity profile based on Fourier [10–13] and Gaussian [14,15] basis expansion functions have also been proposed.

The basic quantity for an ideal numerical Abel inversion technique should be that it is accurate, stable and computationally efficient. The performance of some inversion techniques has been compared in previous studies [16–18]. Most of the comparison, however, is only limited to the techniques that need filtering the noise in advance of the inversion. Other widely used techniques such as the inversion based on piecewise polynomial least-squares fitting [7–9] and Fourier-Hankel transform [10–13] have not been systematically compared so far. Since experimental data are unavoidably contaminated by noise, it is important to know the performance of different inversion techniques under the practical condition with uncertainties. Only the technique that can yield better results in the case of experimental data with noise will be more valuable.

In this study, I compare the noise property and inversion accuracy of techniques using polynomial interpolation, piecewise polynomial least-squares fitting and Fourier-Hankel transform. For the technique without noise resisting property, noise in the projection data was filtered by using different smoothing methods. Under such condition, the performance of all the inversion techniques can be compared fairly. In the following sections, we first describe the different inversion techniques, then analyze and compare the noise property and accuracy of these techniques, and at last show an example of the techniques being applied to experimental data.

2. Numerical Abel inversion methods

As the intensities measured are always in sets of discrete data, it is convenient to take the inversion using a discrete method that directly connects the studied values to the experimentally obtained intensities by a two-dimensional matrix, namely

$$\varepsilon(r_i) = \frac{1}{\Delta r}\sum_{j=0}^{N} D_{ij}I(x_j), \tag{3}$$

where N is the number of the projection data on one side of the source, $r_i = i\Delta r\ (i = 0,1,\ldots,N)$, $x_j = j\Delta x\ (j = 0,1,\ldots,N)$, and $\Delta r = \Delta x = R/N$. Since for the reconstruction of $\varepsilon(r_i)$ only a single summation is performed, the reconstruction speed will be fast if the inversion matrix D_{ij} is calculated in advance. As shown in the following, most of the inversion techniques can be written in the form of Eq. (3).

2.1. *Third-degree polynomial interpolation technique*

The method proposed by Bockasten [5] has a higher accuracy compared with other polynomial interpolation based techniques. In Bockasten's paper, the intensity profile at each interval between two adjacent data points was represented by a cubic polynomial. For the interval near the source center the constraint $I'(0) = 0$ was applied, and the intensity profile in the edge interval was approximated with a second-degree polynomial. Only part of the expressions for calculating the inversion

Email: shlgma@126.com (Shuiliang Ma).

matrix D_{ij} is presented in [5]. For convenience, we write the inversion matrix as

$$D_{ij}=\begin{cases}0, & 2\le i\le N-1, 0\le j\le i-2,\\ U_0(i,j), & 1\le i\le N-1, j=i-1,\\ U_1(i,j), & 0\le i\le N-1, j=i,\\ U_2(i,j), & 0\le i\le N-2, j=i+1,\\ U_3(i,j), & 0\le i\le N-3, i+2\le j\le N-1,\end{cases} \tag{4}$$

where

$$U_m(i,j)=-\frac{1}{\pi}\sum_{l=0}^{m}\sum_{k=0}^{2}\theta_{lk}^{j-l+1}\int_{j-l+1}^{j-l+2}\frac{t^k\mathrm{d}t}{\sqrt{t^2-i^2}}, \tag{5}$$

with θ_{lk}^{j} the elements of matrix Θ_j. For $1\le j\le N-2$,

$$\Theta_j=\begin{bmatrix}-(3j^2+6j+2)/6 & j+1 & -1/2\\ (3j^2+4j-1)/2 & -3j-2 & 3/2\\ -(3j^2+2j-2)/2 & 3j+1 & -3/2\\ (3j^2-1)/6 & -j & 1/2\end{bmatrix}, \tag{6}$$

and for $j=0$ and $N-1$, respectively,

$$\Theta_0=\begin{bmatrix}0 & 0 & 0\\ 0 & -7/2 & 9/4\\ 0 & 4 & -3\\ 0 & -1/2 & 3/4\end{bmatrix},\quad \Theta_{N-1}=\begin{bmatrix}-N+1/2 & 1 & 0\\ 2N-2 & -2 & 0\\ 0 & 0 & 0\\ 0 & 0 & 0\end{bmatrix}. \tag{7}$$

The integration in Eq. (5) has an analytical expression, thus D_{ij} can be easily calculated.

2.2. *Versatile polynomial fitting technique*

In a more general case, the intensity profile can be represented by piecewise polynomials. Considering separating the whole interval $[0,R]$ into K segments, $I(x)$ can be approximated as [9]

$$I(x)\simeq\sum_{n=1}^{K}\omega_n(x)P_{nM}(x)=\sum_{n=1}^{K}\omega_n(x)\sum_{m=0}^{M}a_{nm}x^m, \tag{8}$$

where $\omega_n(x)=1$ for $x_{n-1}\le x\le x_n$ and $\omega_n(x)=0$ otherwise, and $P_{nM}(x)$ is a polynomial of degree M defined over $[x_n^a, x_n^b]$ with $x_n^a\le x_{n-1}<x_n\le x_n^b$. The overlapping factor is defined as $\rho=(x_n^b-x_n^a)/R$. Substituting Eq. (8) into Eq. (2) and with some simplifications, we have

$$\begin{aligned}\varepsilon_k(r) =& -\frac{1}{\pi R}\sum_{n=k}^{K}\sum_{m=1}^{M}ma_{nm}\Big[\delta_{nk}\int_{r}^{x_n}\frac{x^{m-1}}{\sqrt{x^2-r^2}}\mathrm{d}x\\ &+(1-\delta_{nk})\int_{x_{n-1}}^{x_n}\frac{x^{m-1}}{\sqrt{x^2-r^2}}\mathrm{d}x\Big],\end{aligned} \tag{9}$$

where $1\le k\le K$, $x_{k-1}\le r\le x_k$, $\varepsilon_k(r)$ is the expression of the emission coefficient for the kth segment, δ_{nk} is the Kronecker δ-function, and the interval $[0,R]$ is normalized to $[0,1]$, i.e., $x_0=0$ and $x_K=1$. Eq. (9) is called the versatile polynomial fitting (VPF) method.

The fitting coefficients a_{nm} in Eq. (9) can be calculated as follows. With $f_{nl}(x)$ as orthogonal polynomial basis functions, $P_{nM}(x)$ can be expanded as

$$P_{nM}(x)=\sum_{l=0}^{M}c_{nl}f_{nl}(x)=\sum_{l=0}^{M}\sum_{m=0}^{l}c_{nl}d_{nlm}x^m, \tag{10}$$

where

$$c_{nl}=\int_{x_n^a}^{x_n^b}f_{nl}(x)I(x)\mathrm{d}x, \tag{11}$$

$$f_{nl}(x)=\sqrt{\frac{2l+1}{x_n^b-x_n^a}}P_l\left(\frac{2x-x_n^b-x_n^a}{x_n^b-x_n^a}\right), \tag{12}$$

with d_{nlm} the coefficient of x^m in $f_{nl}(x)$ and $P_l(y)$ the Legendre polynomial [19] of degree l defined over $[-1,1]$. Taking an exchange in the order of summation in Eq. (10) and comparing with Eq. (8), one obtains

$$a_{nm}=\sum_{l=m}^{M}c_{nl}d_{nlm}. \tag{13}$$

The value of c_{nl} was calculated based on Eq. (11) with the assumption that the intensity data $I(x)$ is one period of a periodic function. More details can be found in [8].

The performance of the VPF method is determined by several parameters, such as the number of segments, the degree of the polynomial in each segment, and the length of the segment for approximation (the overlapping factor ρ). It is found that in most cases good results can be obtained with $K=5$, $M=6$, and varying the value of ρ [9].

2.3. *Fourier transform based techniques*

Provided the intensity function $I(x)$ in Eq. (1) is symmetric and continuous, it may be expanded as a summation of cosine basis functions [10]:

$$I(x)=a_0+\sum_{k=1}^{\infty}a_k\cos\left(\frac{k\pi x}{R}\right), \tag{14}$$

where a_k are the Fourier expansion coefficients. Substituting Eq. (14) into Eq. (2), we get

$$\varepsilon(r)=\frac{\pi}{2R}\sum_{k=1}^{\infty}k\,a_k\,g(k\pi/R,r,R), \tag{15}$$

where

$$g(\omega,r,R)=\frac{2}{\pi}\int_{r}^{R}\frac{\sin(\omega x)}{\sqrt{x^2-r^2}}\mathrm{d}x. \tag{16}$$

Note that the lower limit of the integration is singular and an oscillate term exists, thus the value of $g(\omega,r,R)$ is difficult to calculate.

If the source radius $R\to\infty$, then $g(\omega,r,R)\to J_0(\omega r)$ and the summation in Eq. (15) should be replaced by integration, Eq. (15) becomes

$$\varepsilon(r)=\frac{1}{2\pi}\int_{0}^{\infty}G(\omega)\omega J_0(\omega r)\mathrm{d}\omega, \tag{17}$$

where $G(\omega)$ is the continuous Fourier transform of $I(x)$ and $J_0(\omega r)$ is the zero-order Bessel function of the first kind [20]. By taking the Fourier transform of $I(x)$ of Eq. (1) and changing the variables of integration to polar coordinates, it can be shown that the Fourier transform of $I(x)$ is equal to the zero-order Hankel transform of $\varepsilon(r)$. Therefore, Eq. (17) can also be obtained from the inverse Hankel transform of $G(\omega)$. This is the so-called Fourier-Hankel transform method.

With frequency spacing $\Delta\omega=\alpha\pi/R$, Eq. (17) can be discretized as

$$\varepsilon(r_i)=\frac{\alpha^2\pi}{2NR}\sum_{k=1}^{N}k\,G(\alpha k)J_0\left(\frac{\alpha ik\pi}{N}\right), \tag{18}$$

where

$$G(\alpha k)=\sum_{j=-N}^{N-1}I(x_j)\cos\left(\frac{\alpha jk\pi}{N}\right). \tag{19}$$

The value of α should be ≤ 1 to make sure the Nyquist criteria [21] is satisfied. Decreasing the value of α means interpolation of $I(x)$ in frequency domain which is equivalent to padding zeros in space domain. Thus the radius of the source is extended from R to R/α with the value of α being changed from 1 to α. Eq. (17) is valid only for $R \to \infty$. To make this condition be approximately satisfied, a small value of α should be used and at the same time all the Fourier components should be reserved. In this case, the discretized form of Eq. (17) is modified as [13]

$$\varepsilon(r_i) = \frac{\alpha^2 \pi}{NR} \sum_{j=0}^{N} \omega_j I(x_j) \sum_{k=1}^{\lfloor \eta N/\alpha \rfloor} k J_0\left(\frac{\alpha i k \pi}{N}\right) \cos\left(\frac{\alpha j k \pi}{N}\right), \tag{20}$$

where $\omega_j = 0.5$ for $j = 0$ and N and $\omega_j = 1$ otherwise, $\lfloor y \rfloor$ denotes the nearest integer $\leq y$, and η is a smoothing factor on the interval $(0, 1]$. Eq. (20) is called the modified Fourier-Hankel (MFH) method.

3. Noise property

3.1. *Theoretical analysis*

The singularity and the derivative of projection in Abel inversion will cause a larger uncertainty in the reconstructed value towards the center of the source. This can be analyzed with the assumption that the noise in the intensity data satisfies $I'(x) = 1$. According to Eq. (2) ($R = 1$) and with $t = (x^2 - r^2)^{1/2}$, we have

$$\varepsilon(r) \sim \int_0^{\sqrt{1-r^2}} \frac{\mathrm{d}t}{\sqrt{t^2 + r^2}} = \operatorname{asinh}\sqrt{r^{-2} - 1}. \tag{21}$$

The radial distribution of the amplified noise is shown in Fig. 1. It is clear to see that the inversion uncertainty increases towards the source center. This, as the intrinsic property of Abel inversion, indicates that any numerical methods will encounter the same problem. It is also clear that only in the most inner 10% interval the uncertainty increases rapidly, so the results in the outer 90% interval will still be reliable.

To reduce the uncertainties in the reconstructed results due to the existence of noise, it is important to know the effect of noise in different frequencies. Assume that the noise can be described by $I(x) = k^{-1/2}\cos(2\pi k x)$ and based on Eq. (2) ($R = 1$), one obtains [22]:

$$\varepsilon(0) = 2\sqrt{k} \int_0^k \frac{\sin(2\pi\zeta)}{\zeta} \mathrm{d}\zeta \sim \pi\sqrt{k}, \quad \zeta = kx. \tag{22}$$

This equation shows that a higher frequency noise will generate higher uncertainties in the source center. The investigation

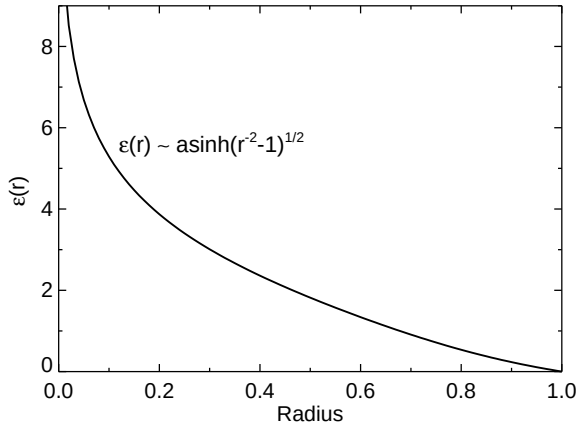

Fig. 1. Radial distribution of inversion uncertainties due to the singularity and derivative in Abel inversion. The uncertainty increases rapidly towards the source center, but only the most inner 10% region is very sensitive to noise.

of band-limited white noise also shows that the high frequency noise components will cause a higher uncertainty in the reconstructed values and the uncertainty becomes larger towards the source center [23]. Since most measured signals can be approximated by a few low frequency components of the Fourier expansion, the higher frequency components that are dominated by noise should be removed to reduce the effect of noise for inversion techniques without smoothing function.

3.2. *Numerical comparisons*

All the inversion techniques presented in Sec. 2 can be written in the matrix form of Eq. (3), so the noise amplification property of these techniques can be directly compared without knowing the shape of the projection profiles. If the derivative of the noise in each projection is the same and independent of the data positions, the noise coefficient that represents the sensitivity of the inversion technique to noise can be expressed as [5,17,18]

$$\beta_i = \left(\sum_{j=0}^{N} D_{ij}^2\right)^{1/2}. \tag{23}$$

Figs. 2(a-c) and (d-f) show, respectively, the inversion coefficients D_{ij} at $i = 4$ with $N = 10$ and the noise coefficients for different inversion techniques with $N = 100$. In Figs. 2(a) and (d), for the VPF method $K = N$, $M = 3$, and $\rho = 3/N$ and for the MFH method $\alpha = 0.01$ and $\eta = 1$. Since the Nestor-Olsen method [4] is very simple and the 3-point technique presented by Dasch [17] shows better performance than other methods, these two techniques are also included in Fig. 2 for a comparison. The inversion coefficients for different techniques shown in Fig. 2(a) have the same characteristic: the terms D_{ii} and $D_{i,i+1}$ have different signs; this forms the derivative operator in the Abel inversion. The higher value in D_{ii} and lower value in $D_{i,i+1}$ imply that this method is more sensitive to noise. Therefore, according to the inversion coefficients it is clear that the Nestor-Olsen method is most sensitive to noise and the 3-point technique least, which are consistent with the results shown in Fig. 2(d).

Figs. 2(b,e) and (c,f) show, respectively, the results for the VPF and MFH methods, which have smoothing property. For the VPF method, we use $K = 5$, $M = 6$, and different values of ρ. As ρ increases, the inversion coefficient distribution expands and the amplitude decreases, the inversion method thus becomes less sensitive to noise. The noise coefficients in Fig. 2(e) show the same results. For $\rho = 0.2$, it is obvious that the inverted profile will have much higher errors in regions near both ends of each least-squares fitting interval (known as termination error). When $\rho > 1/K = 0.2$, a few points near both ends of the approximation interval are not used for the inversion, thus the termination error is avoided and the noise coefficient profile becomes smoother. For the MFH method, we use $\alpha = 0.01$ and several values of η. As η decreases, the inversion coefficient distribution expands and the method becomes less sensitive to noise, which are the same as those of the VPF method.

4. Inversion accuracy

A good inversion technique should be insensitive to noise and have a relatively high accuracy. Although the noise amplification property of different Abel inversion techniques can be compared directly, the accuracy of these techniques is still unknown. To compare the inversion accuracy, it is desirable to use simulated data as the exact solution is known. For this

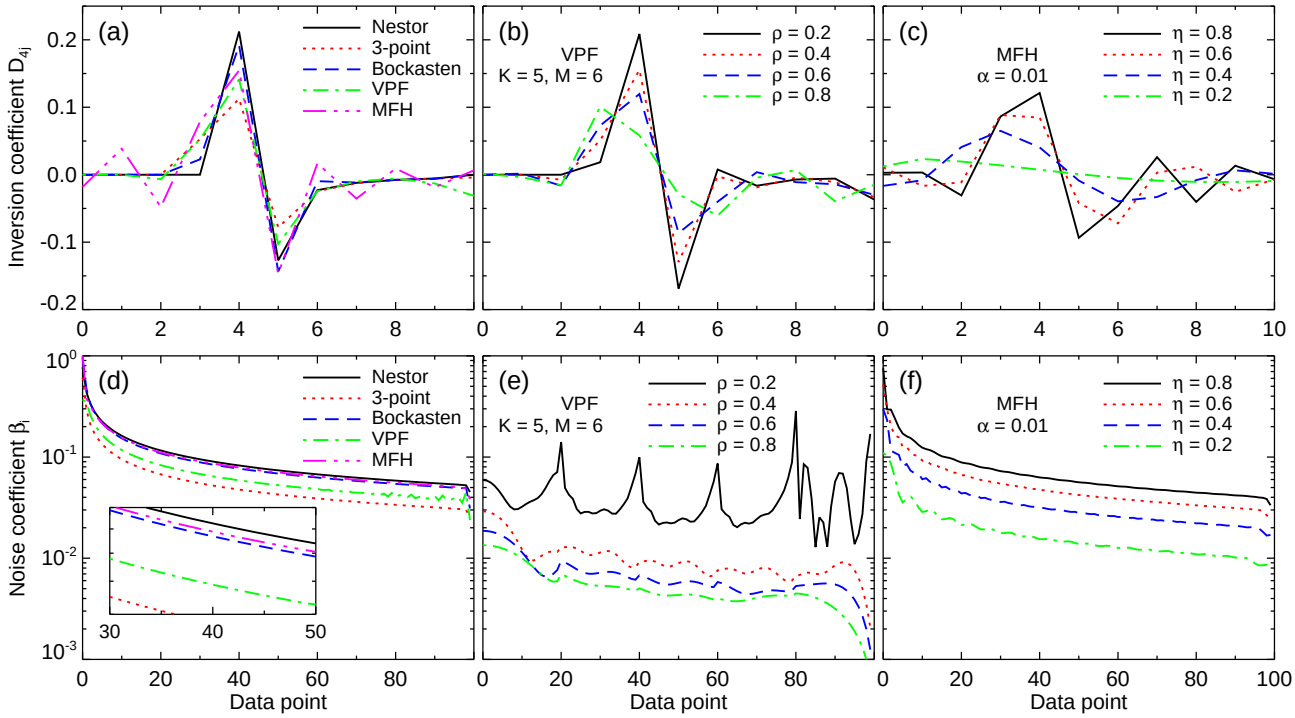

Fig. 2. (Color online) (a-c) Inversion coefficients with $N = 10$ and (d-f) noise coefficients with $N = 100$ for different Abel inversion techniques: (a,d) inversion techniques without noise resisting property, for the VPF method $K = N$, $M = 3$, and $\rho = 3/N$ and for the MFH method $\alpha = 0.01$ and $\eta = 1$, (b,e) the VPF method with $K = 5$, $M = 6$, and several overlapping factors ρ, and (c,f) the MFH method with $\alpha = 0.01$ and different smoothing factors η.

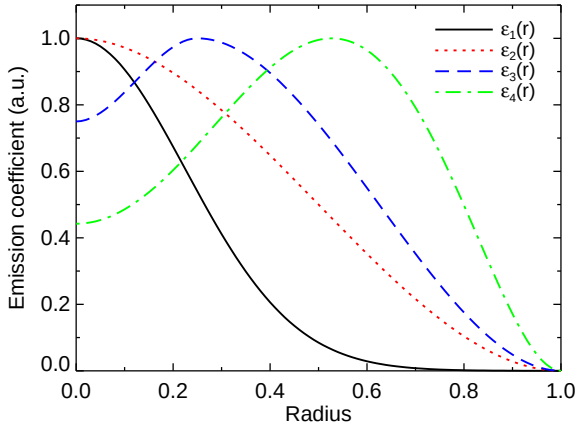

Fig. 3. (Color online) Radial distributions of the emission coefficient for four test profiles.

purpose, four test profiles with various shapes are chosen from numerous examples in the literature [7,22,24]:

$$\varepsilon_1(r) = \exp[-(\pi r)^2], \quad 0 \le r \le 1, \tag{24}$$

$$\varepsilon_2(r) = (1-r)^2(1+2r), \quad 0 \le r \le 1, \tag{25}$$

$$\varepsilon_3(r) = \frac{3}{4} + 12r^2 - 32r^3, \quad 0 \le r \le 0.25,$$
$$= \frac{16}{27}(1-r)^2(1+8r), \quad 0.25 < r \le 1, \tag{26}$$

and

$$\varepsilon_4(r) = (1-r^2)^2(1+12r^2)/(2197/972), \quad 0 \le r \le 1. \tag{27}$$

The radial emission coefficient distributions of these profiles are shown in Fig. 3. The shape of the test profiles changes from the Gaussian function to the off-axis peak distribution, which are commonly encountered in plasma diagnostics.

The intensity data $I_1(x)$ to $I_4(x)$ needed as the input of the inversion are obtained by direct integration of Eq. (1). Experimental additive uncertainties are simulated with normally distributed random noise with an absolute scale independent of the test profiles being imposed on the intensity data. To estimate the inversion performance, the absolute inversion error at each data point is calculated by

$$\Delta\varepsilon(r_i) = \varepsilon_t(r_i) - \varepsilon_c(r_i), \tag{28}$$

where $\varepsilon_t(r_i)$ and $\varepsilon_c(r_i)$ are, respectively, the theoretical and calculated emission coefficients at point r_i. The standard deviation σ is also calculated:

$$\sigma = \left\{ \frac{1}{N} \sum_{i=0}^{N-1} [\varepsilon_t(r_i) - \varepsilon_c(r_i)]^2 \right\}^{1/2}. \tag{29}$$

Considering that the off-axis peak distribution is much more difficult to reconstruct faithfully than other types of distributions such as $\varepsilon_1(r)$ and $\varepsilon_2(r)$, we use $\varepsilon_4(r)$ to test the inversion accuracy of different numerical techniques. Figs. 4(a-c) and (d-f) show the inversion accuracies of the techniques without noise suppressing property and the VPF and MFH methods for intensity data $I_4(x)$ with different numbers of data points N, respectively, without and with noise. The level of noise in the intensity data was $S = 0.03$.

Figs. 4(a) and (d) show the standard deviations of the inversion using techniques without noise suppressing property. It is clear to see that the method which has a higher accuracy for noise free data is more sensitive to noise, except the Nestor-Olsen method which has the lowest inversion accuracy for noise free data but is more sensitive to noise than the 3-point and VPF methods. The VPF method is superior to the 3-point technique for data with or without noise. Bockasten's method and the MFH method have the highest accuracies for data without noise; the MFH method is a little superior to Bockasten's method. As the number of data points N increases, the inversion accuracy increases for noise free data, while the inversion accuracy decreases for data with noise. The big difference between the inversions with and without noise indicates that there is a large space to improve the inversion accuracy by reducing

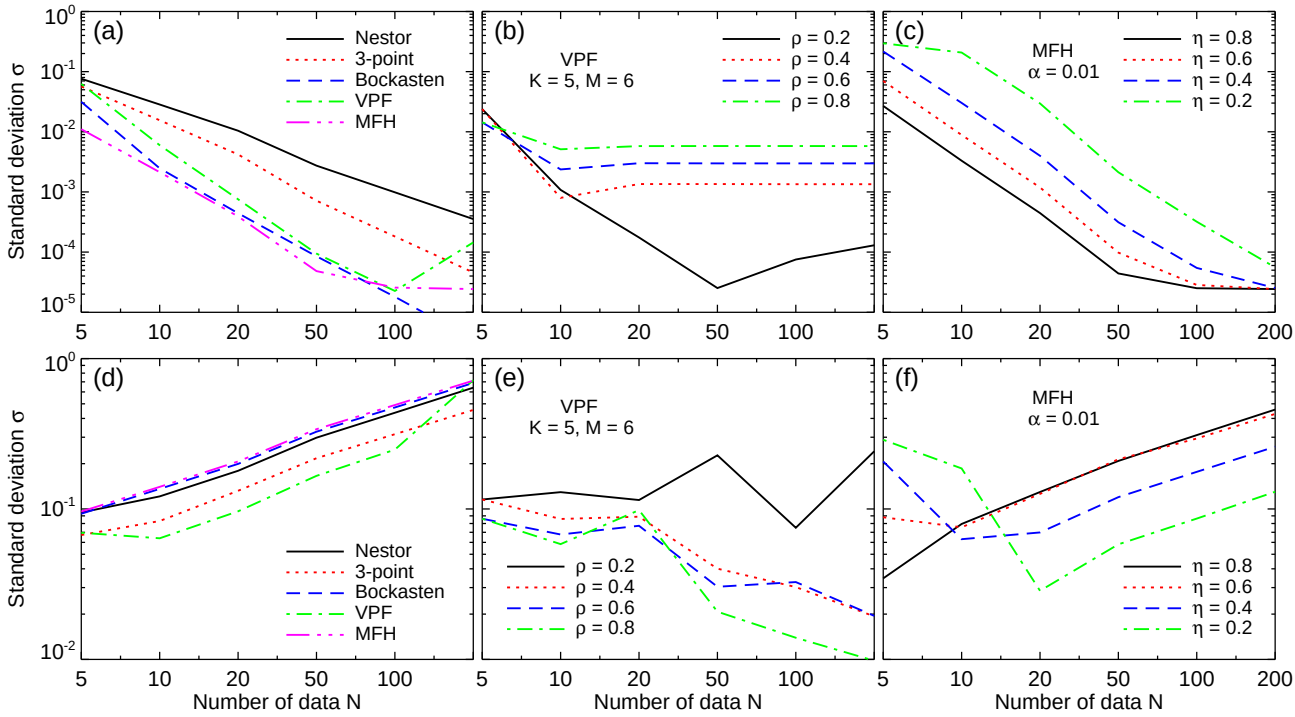

Fig. 4. (Color online) Standard deviations for different inversion techniques with various values of N (5, 10, 20, 50, 100, and 200) for $I_4(x)$: (a-c) noise free data and (d-f) noisy data with $S = 0.03$. Other conditions are the same as Fig. 2.

the effect of noise. Therefore, for the technique without noise suppressing property, a good smoothing method that will effectively reduce the influence of noise is more important than the accuracy of the technique itself.

Figs. 4(b) and (e) show the standard deviations of the inversion using the VPF method with $K = 5$, $M = 6$ and several values of ρ. For noise free data, σ increases with the increase of ρ and is almost independent of N. While for noisy data, σ is not very sensitive to the overlapping factor and improves significantly for $N \geq 50$. Figs. 4(c) and (f) show the results obtained by the MFH method with $\alpha = 0.01$ and different smoothing factors. As expected, with the decrease of η the ideal inversion accuracy decreases. In the case of data with noise, σ first decreases and then increases with the increase of N. For fixed values of η, as N increases more high frequency components of the Fourier transform are reserved, which are dominated by noise, thus σ increases. As N decreases, fewer low frequency components are reserved and the intensity profile is distorted, thus σ increases rapidly. This suggests that it is possible to optimize the smoothing factor to obtain the optimum inversion results for different values of N.

Comparing the results from the three kinds of inversion technique, it is seen that for noise free data the techniques without noise suppression property yield the best performance, while for noisy data almost all techniques yield results with σ higher than the standard deviation of the noise. In Fig. 4(d), even for $N \leq 10$, σ increases with the increase of N, indicating that the effect of noise is more significant than the numerical error. Thus for such sparse data, the VPF and MFH methods still have the potential to give a higher inversion accuracy. For larger values of N, both the VPF and MFH methods can more effectively reduce the influence of noise and for the techniques without noise resisting property, filtering of noise can also be easily implemented. Therefore, when it is possible the number of data points should be ≥ 50 for obtaining better inversion results.

For techniques without noise suppressing property, the intensity data should be smoothed before the inversion. Many noise filtering methods such as the Savitzky-Golay filter, the Gaussian filter, and the Blackman window have been used for smoothing data in Abel inversion [12] and in Langmuir probe measurement [25]. It is shown that the Gaussian and Blackman filters have similar performance and are superior to other filters [12,25]. Based on this fact, we use both the Gaussian and Blackman filters to smooth the data for Bockasten's method, and compare the inverted results with those from the VPF and MFH methods. The Gaussian filter function is given by [25,26]

$$g_n(x) = \sum_{k=1}^{n} \binom{n}{k} (-1)^{k+1} \frac{1}{\sigma\sqrt{2\pi k}} \exp\left(-\frac{x^2}{2\sigma^2 k^2}\right), \qquad (30)$$

where n is the number of iterations and σ is the standard deviation. It is found that $n = 1$ gives the best results, so only adjusting the value of σ is needed to control the smoothing degree. The Blackman window is given by [25]

$$f_B(n) = 0.42 - 0.5\cos\left(\frac{2\pi n}{w}\right) + 0.08\cos\left(\frac{4\pi n}{w}\right), \qquad (31)$$

where $n = 0, 1, 2, \cdots, w$ and w is the size of the window used for controlling the smoothing degree.

Fig. 5(a) shows the theoretical intensity profile $I_4(x)$, the intensity data added normally distributed noise with $S = 0.05$, and the profiles smoothed with the Gaussian and Blackman filters. Fig. 5(b) shows the corresponding theoretical emission coefficient profile $\varepsilon_4(r)$ and the profiles inverted using Bockasten's method with the Gaussian and Blackman filters as well as using the VPF and MFH methods for the noisy intensity profile without filtering noise. The radial distributions of the absolute inversion error for these methods are presented in Fig. 6. The number of data points is 100. All the methods use the optimum smoothing parameters: for the Gaussian filter $\sigma = 4.8$, for the Blackman filter $w = 30$, for the VPF method $\rho = 1.1$, and for the MFH method $\eta = 0.05$. The intensity profile is treated as one period of a periodic function to avoid edge effect when using filters to suppress noise. We see that the Gaussian and

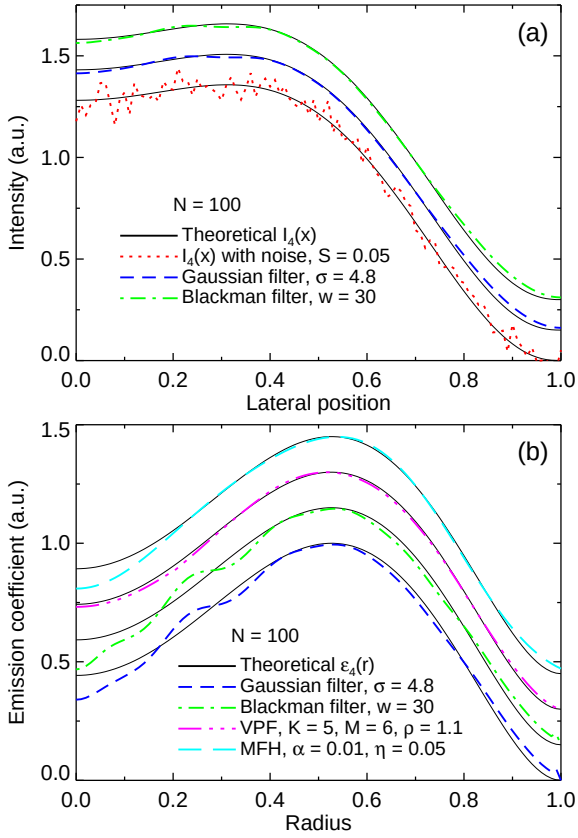

Fig. 5. (Color online) (a) Intensity profiles of $I_4(x)$ without noise, added noise with $S = 0.05$, and smoothed with the Gaussian filter ($\sigma = 4.8$) and the Blackman filter ($w = 30$). (b) Corresponding theoretical emission coefficient profile and the profiles inverted with Bockasten's method for $I_4(x)$ smoothed by the Gaussian and Blackman filters and those inverted with the VPF ($K = 5$, $M = 6$, and $\rho = 1.1$) and MFH ($\alpha = 0.01$ and $\eta = 0.05$) methods. The number of data points is 100. Each profile is offset from the nearest one for clarity.

Blackman filters yield almost identical results. Compared with the inversion with noise filters, the VPF and MFH methods give markedly better results. Note that all methods have negative errors near the source center and positive errors near the edge. More tests indicate that the negative errors near the center are due to the distribution of noise, whereas the positive errors near the edge are due to the smoothing effect. The Gaussian and Blackman filters that smooth the noise in the data profile also smooth the variation of the intensity profile, thus the noise is difficult to be removed effectively. On the other hand, the VPF and MFH methods can more effectively decrease the effect of noise and are less likely to distort the shape of the intensity profile. Tests with many other random noise distributions also demonstrate that the VPF and MFH methods have higher inversion accuracies compared with techniques using the Gaussian and Blackman noise filters.

Since the VPF and MFH methods give better results than the smoothing filters, we test only these two methods for profiles $\varepsilon_1(r)$ to $\varepsilon_4(r)$ with noise of $S = 0.005$ and 0.02 and different numbers of data points. In order to compare the noise reducing performance, the smoothing parameters for the VPF and MFH methods are optimized.

The optimum overlapping factors ρ for the VPF method are presented in Fig. 7. Apparently, the value of ρ is dependent on the test profile shapes. For a higher level of noise, a larger ρ will give a better inversion, because for the least-squares fitting the fitting performance depends on the number of data points and the noise level. It is found that the inversion accuracy is not very sensitive to ρ. In most cases, the results have minor

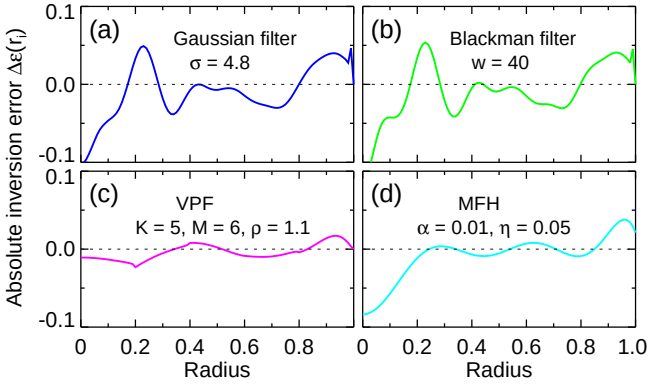

Fig. 6. (Color online) Radial distributions of the absolute inversion error for $I_4(x)$ with noise of $S = 0.05$: (a) Bockasten's method with the Gaussian filter, (b) Bockasten's method with the Blackman filter, (c) the VPF method, and (d) the MFH method. Other conditions are the same as Fig. 5.

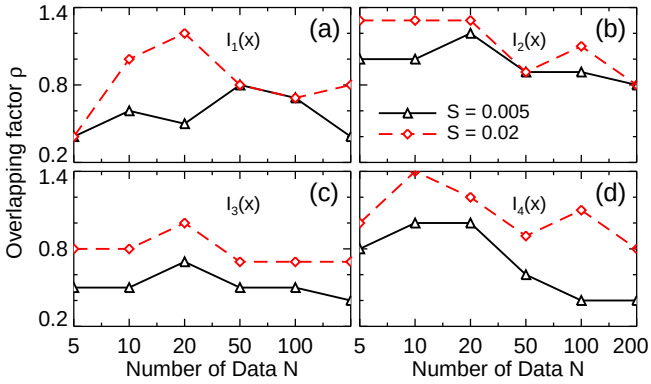

Fig. 7. (Color online) Optimized overlapping factors ρ for the VPF method applied to $I_1(x)$ to $I_4(x)$ with noise of $S = 0.005$ and 0.02 and several values of N.

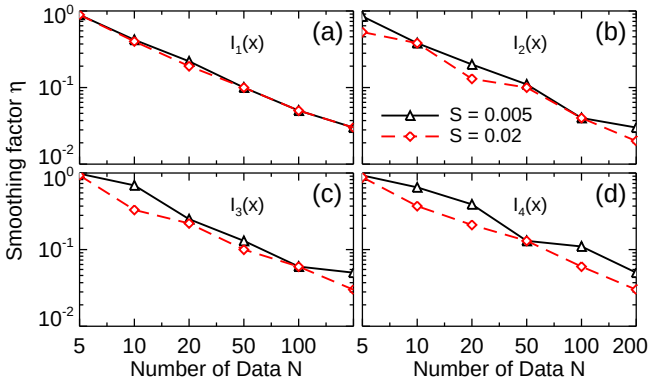

Fig. 8. (Color online) Optimized smoothing factor η for the MFH method applied to $I_1(x)$ to $I_4(x)$ with noise of $S = 0.005$ and 0.02 and several values of N.

changes for a wide range of ρ, which can also be seen from the results shown in Fig. 4(e).

The optimum smoothing factors η for the MFH method are presented in Fig. 8. It is not the same as the case in the VPF method, η is less dependent on the shape of the test profiles. Since each profile can be approximated by a few low frequency components of the Fourier transform, the optimum η is almost inversely proportional to N. As the level of noise increases, the frequency at which the noise is comparable with the signal deceases, thus the optimum value of η should also be lowered. The value of η usually has a narrow range: when η is too large, the influence of noise cannot be efficientlyeffectively reduced; when η is too low, the profile will be distorted.

Based on the optimized smoothing parameters, the standard

Table 1
Standard deviations of the inversion using the VPF ($K = 5$, $M = 6$) and MFH ($\alpha = 0.01$) methods obtained for $I_1(x)$ to $I_4(x)$ with noise in the level of $S = 0.005$ and 0.02. The overlapping factors ρ for the VPF method and the smoothing factors η for the MFH method are taken from Figs. 7 and 8, respectively.

	$I_1(x)$		$I_2(x)$		$I_3(x)$		$I_4(x)$	
N	VPF	MFH	VPF	MFH	VPF	MFH	VPF	MFH
	$S = 0.005$							
5	1.6E-2	9.0E-3	9.9E-3	5.6E-3	1.3E-2	1.1E-2	1.9E-2	1.2E-2
10	1.3E-2	8.7E-3	8.6E-3	7.9E-3	1.2E-2	1.1E-2	8.2E-3	1.2E-2
20	1.2E-2	1.1E-2	6.3E-3	5.8E-3	9.4E-3	8.6E-3	9.2E-3	1.2E-2
50	4.9E-3	3.1E-3	3.2E-3	3.2E-3	6.1E-3	3.9E-3	5.6E-3	5.0E-3
100	4.7E-3	2.3E-3	2.8E-3	2.5E-3	4.1E-3	5.3E-3	5.3E-3	4.8E-3
200	3.2E-3	1.8E-3	2.4E-3	1.8E-3	3.2E-3	3.0E-3	3.6E-3	3.1E-3
	$S = 0.02$							
5	5.7E-2	2.9E-2	2.7E-2	1.8E-2	4.0E-2	2.7E-2	4.0E-2	2.5E-2
10	4.3E-2	3.3E-2	3.0E-2	3.1E-2	3.9E-2	3.9E-2	2.3E-2	3.4E-2
20	4.3E-2	3.1E-2	1.5E-2	8.5E-3	1.6E-2	2.1E-2	1.7E-2	2.2E-2
50	1.1E-2	1.2E-2	8.6E-3	1.2E-2	1.7E-2	1.6E-2	1.1E-2	1.5E-2
100	1.2E-2	8.2E-3	5.7E-3	7.8E-3	9.8E-3	9.9E-3	7.2E-3	1.1E-2
200	8.5E-3	7.0E-3	5.8E-3	5.8E-3	9.9E-3	8.4E-3	7.9E-3	9.8E-3

deviations of the inversion for the test profiles $I_1(x)$ to $I_4(x)$ are listed in table 1. The VPF and MFH methods yield comparable results for all the test profiles. With the increase of N, the inversion accuracy increases. For $N \geq 50$, the influence of noise is effectively suppressed: the standard deviation of the inversion is smaller than that in the noise. Considering that both of the two methods can generate quite good results, it is better to use the two methods to crosscheck the inversion in practical application.

5. Application to experimental data

All inversion techniques should ultimately be used in practice, thus the performance of the VPF and MFH methods are further tested with experimental data. We use the intensity profiles measured from several layers of a free-burning arc plasma with distances of 0.5, 1.5, 2.5, and 3.5 mm from the arc cathode tip [9]. As shown in Fig. 9(a), these intensity profiles have different shapes from the bell distribution to the off-axis peak distribution, and thus are very suitable for the test. The number of data points for these profiles is 40, 50, 60, and 60, respectively. Since the number of data points is large enough, no interpolation was used on the intensity profiles. The noise in the measured data was estimated to have a standard deviation of $S = 0.007$, with the assumption that the higher frequency components in the frequency domain is dominated by noise.

The difficulty for the VPF and MFH methods is that there is no theoretical criterion for the determination of the smoothing parameters (it is also true for most smoothing techniques). Therefore, these smoothing parameters have to be determined empirically. We find that, for the VPF method, the inversion accuracy is not very sensitive to the overlapping factor. With the increase of noise level, the overlapping factor has to be increased to more effectively suppress noise. Based on the experimental noise level, we guess a first value and take the inversion. We then increase or decrease the guessed value to take another inversion. When the two inverted profiles are smooth and the difference between them is negligible, the value between the two overlapping factors is considered as the optimum overlapping factor. In this way, the overlapping factor for the VPF method is determined as 0.35. On the other hand, the determination of the smoothing factors for the MFH method is much straightforward. First, we take the Fourier transform of the projection data. Then, we observe the frequency spectrum

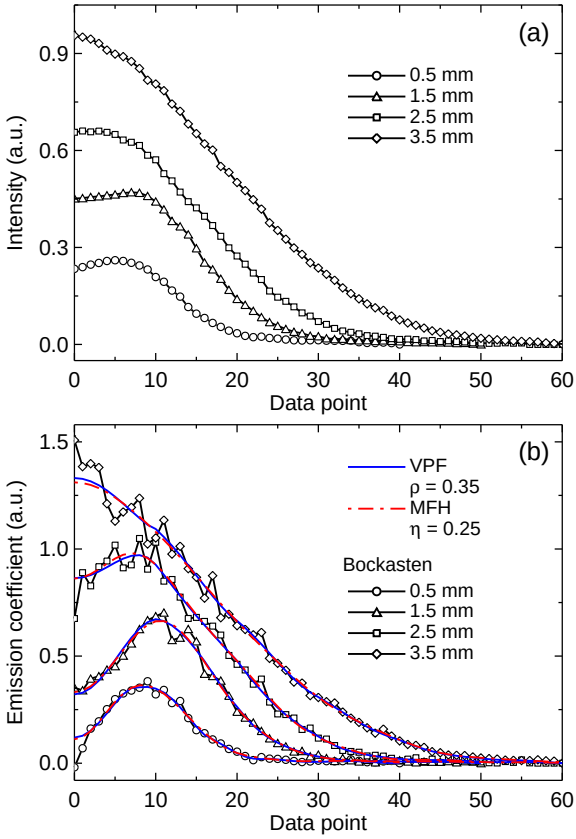

Fig. 9. (Color online) Distributions of (a) experimental intensities measured from different layers of an arc plasma, and (b) the corresponding radial emission coefficients inverted using Bockasten's method [5], the VPF method with $K = 5$, $M = 6$, and $\rho = 0.35$, and the MFH method with $\alpha = 0.01$ and $\eta = 0.25$.

and determine the cut-off frequency based on the assumption that the frequency components of the projection fall predominantly at low frequencies. The value of the smoothing factor is the ratio between the cut-off frequency and the Nyquist frequency. For relatively low level of noise, it is usually very easy to determine the cut-off frequency. The smoothing factor for the MFH method is estimated as 0.25.

The emission coefficient profiles inverted with the VPF and MFH methods are shown in Fig. 9(b). It is seen that the two methods yield very consistent results. There are only minor differences in the most inner 15% region for the profiles with distances of 2.5 and 3.5 mm from the arc cathode tip. Since inversion techniques without noise suppressing property will not distort the profile distributions, the results from Bockasten's method are also included in Fig. 9(b). The comparison indicates that the emission coefficient profiles inverted using the VPF and MFH methods are not distorted, and thus the results obtained are reliable. With the results from Bockasten's method as a reference, it is also useful to determine the optimum smoothing parameters for the VPF and MFH methods, i.e., the optimum smoothing parameter should ensure that the inverted profiles with the VPF or MFH methods are smooth enough and the differences between these profiles and the inversion with Bockasten's method are uniformly distributed on the positive and negative sides of zero. Overall, the results from the experimental date validate the use of the two proposed methods for Abel inversion without filtering of noise. In the case of a better noise filtering approach is not available, these methods should be considered as the better choice.

6. Conclusions

Noise property and accuracy of three kinds of Abel inversion technique have been analyzed and compared. These techniques can be divided into two categories: methods without noise resisting property (the polynomial interpolation techniques) and those with smoothing function (the VPF and MFH methods). Since the inversion is expressed in a matrix form, the noise property of these techniques can be compared directly based on the noise coefficients without knowing the shape of the projection profiles. All techniques show the same noise amplification characteristic: the inversion uncertainty increases towards the source center, due to the singularity in Abel inversion; only the most inner 10% region has very large uncertainties. A technique that is more sensitive to noise will have a higher accuracy for noise free data. For techniques without noise resisting property, Bockasten's method and the MFH method ($\alpha = 0.01$, $\eta = 1$) have comparable performance and are superior to other methods. Since the standard deviation of the inversion for noise free data is much lower than that of noise, the accuracy of these techniques is completely determined by noise filtering approaches. In the case of techniques with noise resisting property, both the VPF and MFH methods can be used by adjusting the smoothing parameters to control the smoothing degree. For very sparse data ($N \leq 10$), in which case filtering of noise is impossible, the VPF and MFH methods can yield results with higher accuracies. For a larger number of data points, the two methods also give better results compared with Bockasten's method using smoothing techniques, such as the Gaussian and Blackman filters. Although the optimum smoothing parameter for the VPF method is dependent on the profile shape and the number of data points, the inversion accuracy is not very sensitive to the value of ρ. The optimum smoothing factor in the MFH method can be determined based on the level of noise in the projection data, but the results are more sensitive to the value of η. Both the VPF and MFH methods should be considered when no better smoothing approaches can be used.

I am grateful to Professor John Howard for his encouragement in this research and a critical reading of the manuscript.

References

[1] S. Ma, Tomography of cylindrical objects: comparison of noise property and accuracy of Abel inversion techniques with and without noise filtering, Appl. Opt. 50 (35) (2011) 6512–6521.

[2] H. R. Griem, Principles of Plasma Spectroscopy, Cambridge University Press, Cambridge, 1997.

[3] A. C. Eckbreth, Laser Diagnostics for Combustion Temperature and Species, 2nd Edition, Vol. 3 of Combustion Science and Technology Book Series, Gordon & Breach, Amsterdam, 1996.

[4] O. H. Nestor, H. N. Olsen, Numerical methods for reducing line and surface probe data, SIAM Rev. 2 (3) (1960) 200–207.

[5] K. Bockasten, Transformation of observed radiances into radial distribution of the emission of a plasma, J. Opt. Soc. Am. 51 (9) (1961) 943–947.

[6] G. N. Minerbo, M. E. Levy, Inversion of Abel's integral equation by means of orthogonal polynomials, SIAM J. Numer. Anal. 6 (4) (1969) 598–616.

[7] C. J. Cremers, R. C. Birkebak, Application of the Abel integral equation to spectrographic data, Appl. Opt. 5 (6) (1966) 1057–1064.

[8] S. Ma, H. Gao, L. Wu, G. Zhang, Abel inversion using Legendre polynomials approximations, J. Quant. Spectrosc. Radiat. Transfer 109 (10) (2008) 1745–1757.

[9] S. Ma, H. Gao, G. Zhang, L. Wu, A versatile analytical expression for the inverse Abel transform applied to experimental data with noise, Appl. Spectrosc. 62 (6) (2008) 701–707.

[10] M. Kalal, K. A. Nugent, Abel inversion using fast Fourier transforms, Appl. Opt. 27 (10) (1988) 1956–1959.

[11] L. M. Smith, D. R. Keefer, S. I. Sudharsanan, Abel inversion using transform techniques, J. Quant. Spectrosc. Radiat. Transfer 39 (5) (1988) 367–373.

[12] R. Álvarez, A. Rodero, M. C. Quintero, An Abel inversion method for radially resolved measurements in the axial injection torch, Spectrochim. Acta B 57 (11) (2002) 1665–1680.

[13] S. Ma, H. Gao, L. Wu, Modified Fourier-Hankel method based on analysis of errors in Abel inversion using Fourier transform techniques, Appl. Opt. 47 (9) (2008) 1350–1357.

[14] V. Dribinski, A. Ossadtchi, V. A. Mandelshtam, H. Reisler, Reconstruction of Abel-transformable images: the Gaussian basis-set expansion Abel transform method, Rev. Sci. Instrum. 73 (7) (2002) 2634–2642.

[15] G. A. Garcia, L. Nahon, I. Powis, Two-dimensional charged particle image inversion using a polar basis function expansion, Rev. Sci. Instrum. 75 (11) (2004) 4989–4996.

[16] R. Piche, Noise-filtering properties of numerical methods for the inverse Abel transform, IEEE Tran. Instrum. Meas. 41 (4) (1992) 517–522.

[17] C. J. Dasch, One-dimensional tomography: a comparison of Abel, onion-peeling, and filtered backprojection methods, Appl. Opt. 31 (8) (1992) 1146–1152.

[18] P. S. Kolhe, A. K. Agrawal, Abel inversion of deflectometric data: comparison of accuracy and noise propagation of existing techniques, Appl. Opt. 48 (20) (2009) 3894–3902.

[19] G. E. Andrews, R. Askey, R. Roy, Special Functions, Cambridge University Press, Cambridge, 1999.

[20] G. N. Watson, Theory of Bessel Functions, Cambridge University Press, New York, 1966.

[21] A. V. Oppenheim, A. S. Willsky, S. H. Nawab, Signals and Systems, 2nd Edition, Prentice Hall, Englewood Cliffs, NJ, 1996.

[22] M. J. Buie, J. T. P. Pender, J. P. Holloway, T. Vincent, P. L. G. Ventzek, M. L. Brake, Abel's inversion applied to experimental spectroscopic data with off axis peaks, J. Quant. Spectrosc. Radiat. Transfer 55 (2) (1996) 231–243.

[23] L. M. Smith, Nonstationary noise effects in the Abel inversion, IEEE Trans. Inform. Theory 34 (1) (1988) 158–161.

[24] G. C.-Y. Chan, G. M. Hieftje, Estimation of confidence intervals for radial emissivity and optimization of data treatment techniques in Abel inversion, Spectrochim. Acta B 61 (1) (2006) 31–41.

[25] F. Magnus, J. T. Gudmundsson, Digital smoothing of the Langmuir probe *I–V* characteristic, Rev. Sci. Instrum. 79 (7) (2008) 073503.

[26] J. I. Fernández Palop, J. Ballesteros, V. Colomer, M. A. Hernández, A new smoothing method for obtaining the electron energy distribution function in plasmas by the numerical differentiation of the *I–V* probe characteristic, Rev. Sci. Instrum. 66 (9) (1995) 4625–4636.